

MESH2IR: Neural Acoustic Impulse Response Generator for Complex 3D Scenes

Anton Ratnarajah
University of Maryland
College Park, USA
jeran@umd.edu

Rohith Aralikatti
University of Maryland
College Park, USA
rohithca@umd.edu

Zhenyu Tang
University of Maryland
College Park, USA
zhy@cs.umd.edu

Dinesh Manocha
University of Maryland
College Park, USA
dmanocha@umd.edu

ABSTRACT

We propose a mesh-based neural network (MESH2IR) to generate acoustic impulse responses (IRs) for indoor 3D scenes represented using a mesh. The IRs are used to create a high-quality sound experience in interactive applications and audio processing. Our method can handle input triangular meshes with arbitrary topologies (2K - 3M triangles). We present a novel training technique to train MESH2IR using energy decay relief and highlight its benefits. We also show that training MESH2IR on IRs preprocessed using our proposed technique significantly improves the accuracy of IR generation. We reduce the non-linearity in the mesh space by transforming 3D scene meshes to latent space using a graph convolution network. Our MESH2IR is more than 200 times faster than a geometric acoustic algorithm on a CPU and can generate more than 10,000 IRs per second on an NVIDIA GeForce RTX 2080 Ti GPU for a given furnished indoor 3D scene. The acoustic metrics are used to characterize the acoustic environment. We show that the acoustic metrics of the IRs predicted from our MESH2IR match the ground truth with less than 10% error. We also highlight the benefits of MESH2IR on audio and speech processing applications such as speech dereverberation and speech separation. To the best of our knowledge, ours is the first neural-network-based approach to predict IRs from a given 3D scene mesh in real-time.

CCS CONCEPTS

• **Computing methodologies** → *Real-time simulation; Interactive simulation; Machine learning; Ray tracing.*

KEYWORDS

room acoustics, sound propagation, speech simulation, cross-modal

ACM Reference Format:

Anton Ratnarajah, Zhenyu Tang, Rohith Aralikatti, and Dinesh Manocha. 2022. MESH2IR: Neural Acoustic Impulse Response Generator for Complex 3D Scenes. In *Proceedings of the 30th ACM International Conference on Multimedia (MM '22)*, October 10–14, 2022, Lisboa, Portugal. ACM, New York, NY, USA, 11 pages. <https://doi.org/10.1145/3503161.3548253>

1 INTRODUCTION

Rapid developments in interactive applications (e.g., games, virtual environments, speech recognition, etc.) demand realistic sound effects in complex dynamic indoor environments with multiple sound sources. Generating realistic sound effects is still a challenging problem because of the geometric and aural complexity of the real-world environment. The geometric complexity is a measure of the number of vertices and faces needed to represent the complex environment as a 3D mesh. The aural complexity depends on the number of sound sources, the number of static and dynamic objects in the environment and the acoustic effects (e.g., early reflection, late reverberation, diffraction, scattering, etc.). The way the sound propagates from a sound source to the listener can be modeled as an impulse response (IR) [41]. We can generate sound effects by convolving the IR with a dry sound. The IRs are used to generate plausible sound effects in many interactive applications used for games and AR/VR: Steam Audio [1], Project Acoustics [2], and Oculus Spatializer [3].

Recently, many machine learning-based algorithms are proposed to synthesize the sounds in musical instruments [28, 31], estimate the acoustic material properties, and model the acoustic effects from finite objects [32, 33, 49, 57]. Neural-network-based IR generators [59, 61] for simple rooms are proposed for speech processing applications (e.g., far-field speech recognition, speech enhancement, speech separation, etc.). FAST-RIR [61] is a GAN-based IR generator that takes shoe-box-shaped room dimensions, listener and source positions, and reverberation time as inputs and generates a large IR dataset on the fly. Gaming applications demand fast IR generators for complex scenes. Complex indoor 3D scenes with furniture can be represented in detail using mesh models. Traditional geometric IR simulators take a 3D scene mesh-model and listener and source positions as inputs and generate realistic environmental sound effects [64]. The complexity of geometric IR simulators increases exponentially with the reflection depth [6] and makes them impractical for interactive applications. No current simulation and

Permission to make digital or hard copies of all or part of this work for personal or classroom use is granted without fee provided that copies are not made or distributed for profit or commercial advantage and that copies bear this notice and the full citation on the first page. Copyrights for components of this work owned by others than the author(s) must be honored. Abstracting with credit is permitted. To copy otherwise, or republish, to post on servers or to redistribute to lists, requires prior specific permission and/or a fee. Request permissions from permissions@acm.org.

MM '22, October 10–14, 2022, Lisboa, Portugal

© 2022 Copyright held by the owner/author(s). Publication rights licensed to ACM.

ACM ISBN 978-1-4503-9203-7/22/10...\$15.00

<https://doi.org/10.1145/3503161.3548253>

learning methods can compute real-time IRs for unseen complex dynamic scenes.

Sound propagation can be accurately simulated using wave-based methods. The wave-based methods solve wave equations using different numerical solvers such as the boundary-element method [79], the finite-difference time-domain simulation [10], etc. The complexity of the wave-based approach grows as the fourth power of the frequency and is limited to static scenes. Geometric acoustic algorithms are a less complex alternative to the wave-based method. Geometric acoustic algorithms can handle complex environments with dynamic objects [43] and multiple sources [66]. However, geometric acoustic methods do not model the low-frequency components of the IRs accurately because of the ray assumption. The sound wave can be treated as a ray when the wavelength of the sound is smaller than the obstacles in the environment. At low frequencies under 500 Hz, the ray assumption is not valid for most scenes and results in significant simulation errors. Hybrid sound propagation algorithms [73, 80] combine IRs from wave-based and geometric techniques to generate accurate IRs in the human aural range for complex dynamic scenes. Generating IRs corresponding to thousands of sound sources at an interactive rate is not possible with the hybrid method because of its complexity.

Main Contributions: We propose a novel learning-based IR generator (MESH2IR) to generate realistic IRs for furnished 3D scenes with arbitrary topologies (i.e., meshes with 2000 faces to 3 million faces) not seen during the training. For a given complex scene, MESH2IR can generate IRs for any listener and source positions. We perform mesh simplification to even handle complex 3D scenes represented using a mesh with millions of triangles. Our mesh encoder network significantly reduces the input data size by transforming the 3D scene meshes into low-dimensional vectors of a latent space. Mesh simplification and its encoder network allow us to handle general 3D scenes meshes with a varying number of faces. We present an efficient approach to preprocess the IR training dataset and show that training MESH2IR on preprocessed dataset gives a significant improvement in the accuracy of IR generation. We also evaluate the contribution of energy decay relief in improving the IRs generated from MESH2IR. We train our MESH2IR on an IR dataset computed using a hybrid sound propagation algorithm [73]. Therefore, the predicted IRs from MESH2IR exhibit good accuracy for both low-frequency and high-frequency components. MESH2IR can generate more than 10,000 IRs for a given indoor 3D scene. We show that our MESH2IR can generate IRs 200 times faster than a geometric acoustic simulator [74] on a single CPU. We evaluate the accuracy of the predicted IRs from MESH2IR using power spectrum and acoustic metrics which characterize the acoustic environment. Our MESH2IR can predict the IRs for unseen 3D scenes during training with less than 10% error in three different acoustic metrics. We also show that far-field speech augmented using the IRs generated from MESH2IR significantly improves the performance in speech processing applications.

2 RELATED WORKS

We first give an overview of IR simulators that can compute IRs at interactive rates in Section 2.1. In Section 2.2, we summarize the deep learning-based algorithms used to predict IRs and describe the

prior learning-based IR generator. We highlight various applications in audio and speech processing that can use the predicted IRs in Section 2.3. Finally, we mention different publicly available indoor 3D scenes datasets and give an overview of prior IR datasets.

2.1 PHYSICS-BASED IR COMPUTATION

Many wave-based, geometric-based, and hybrid interactive IR simulation algorithms have been proposed to simulate IRs for complex scenes [44]. Wave-based and hybrid algorithms precompute the IRs for a static scene and, at runtime, the IR for an arbitrary listener position is calculated by efficient interpolation techniques [48, 58, 80]. These precomputation-based interactive IR simulation algorithms can be used only for static scenes [44]. Geometric-based algorithms are proposed for interactive IR simulation in dynamic scenes [43, 65, 75]. The limitations of geometric-based techniques, such as simulation error at lower frequencies, are inherent in these interactive geometric-based algorithms. There are no general physics-based algorithms known for computing accurate IRs, including low-frequency components, for general dynamic scenes.

2.2 LEARNING-BASED IR COMPUTATION

Recently, neural-network-based methods have been developed to estimate IRs from the reverberant speech signal [70] or from a single image of the environment [38, 69], to translate synthetic IRs to real-word IRs [60], to interpolate IRs [62], and to augment the number of IRs [11, 59]. FAST-RIR is a learning-based IR generator that is trained to generate specular and diffuse reflections for a given empty shoe-box-shaped room. FAST-RIR may not compute low-frequency components of IRs accurately.

2.3 AUDIO PROCESSING USING IR

IRs are used in a wide range of practical applications such as audio-visual navigation [15, 16, 45], acoustic matching [14], sound rendering [66], sound source localization [25], speech enhancement [54], speech recognition [47, 68], and speech separation [7, 29]. In most applications, learning-based networks are trained on large, diverse synthetic datasets and tested in real-world environments [74]. The performance of the deep neural network trained for a particular application is depended on the similarity of the synthetic training dataset and the real-world test environment [59]. Synthetic training datasets are created using IR generators. Therefore, the accuracy of the IR generator plays an important role in practical applications that depends on IRs.

2.4 INDOOR 3D SCENES & IR DATABASES

The indoor 3D scenes can be either captured using RGB-D videos and reconstructed as meshes (real-world scenes) [8, 13, 18] or created by humans using professionally designed software (synthetic models) [21, 27]. The mesh quality in the real-world scene datasets is not as good as the quality of the synthetic models because 3D scene reconstruction with accurate geometric details is challenging with existing computer vision methods and capturing hardware. Among the synthetic model datasets, 3D-FRONT [21] contains large-scale synthetic furnished indoor 3D scenes with fine geometric and texture details. The 3D-FRONT dataset has 6813 CAD houses, where 18,968 rooms are furnished with 13,151 3D furniture objects. The

furniture is placed in varying numbers in meaningful locations in each room (e.g., living room, dining room, kitchen, bedroom, etc.)

The publicly available IR datasets are either recorded in a real-world environments (recorded IR) [12, 26, 40, 71] or generated using IR simulation tools (synthetic IR) [15, 24, 37, 73]. The recorded IR datasets are limited in size (fewer than 5000 IRs) and number of environments (fewer than 10 rooms), and no sufficient information on the recording conditions is provided to train a deep learning model. Synthetic IR datasets like SoundSpaces [15] and GWA [73] contain millions of IRs. The IRs in SoundSpaces is simulated using a geometric acoustic method [64] and GWA dataset contains high-quality IRs computed using a hybrid method.

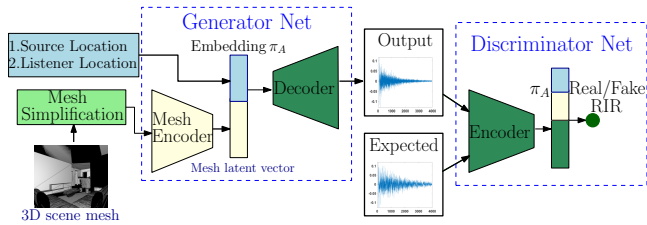


Figure 1: The architecture of our MESH2IR. Our mesh encoder network encodes a indoor 3D scene mesh to the latent space. The mesh latent vector and the source and listener locations are combined to produce a scene vector embedding (π_A). The generator network generates an IR corresponding to the input scene vector embedding. For the given scene vector embedding, the discriminator network discriminates between the generated IR and the ground truth IR during training.

3 MESH2IR: OUR APPROACH

3.1 OVERVIEW

Our goal is to predict the IR for the given indoor 3D scene and the source and listener positions (Equation 1). The 3D scenes are represented as triangular meshes and we do not make any assumptions about the topology of the 3D scenes. The mesh format describes the shape of an object using vertices, edges, and faces consisting of triangles represented using 3D Cartesian coordinates (x, y, z). The source positions and listener positions are also represented using 3D Cartesian coordinates. For each scene material (e.g., furniture, floor, wall, ceiling, etc.), we do not explicitly control the characteristics of the scene materials (the amount of absorption or scattering of sound by the scene material). The IRs used to train our MESH2IR is computed by considering the characteristic of scene material in every indoor 3D scene. Therefore, our trained MESH2IR randomly assigns the characteristics of scene materials based on their shape.

The IR is the response of an impulse signal emitted in an environment. IR describes the relationship between a dry sound and the reflected sound from the boundaries in the scene. The reflected sound signal depends on the scene geometry, scene materials, and source and listener positions. IRs can be accurately simulated by solving the wave equation [10]. However, solving a wave equation is not practical for interactive applications because of its complexity. In our work, we propose a learning-based IR generator (MESH2IR)

that is capable of approximating thousands of IRs per second for a given complex scene. Our network can be formally described as:

$$IR_n = N_{\theta_1}(N_{\theta_2}(M_n), SP_n, LP_n), \quad (1)$$

where IR_n is the predicted IR for the given scene n , M_n is the 3D mesh representation of the scene simplified to have around 2000 faces, LP_n and SP_n are listener location and source location, respectively. LP_n and SP_n are represented using a 3D vector. We simplify the 3D scene mesh with an arbitrary number of faces to have a constant number of faces (2000 faces). We use a mesh-based encoder network N_{θ_2} to transform the simplified 3D mesh into a latent vector of a latent space (Figure 2). N_{θ_1} is a generator network, and θ_1 and θ_2 are the trained network parameters. Our overall network architecture is shown in Figure 1.

In recent years, cross-modal translation neural networks have gained attention in computer vision. Several algorithms have been proposed for translating video to audio [55], image to audio [69], text to image [81, 82], image to mesh [77], etc. In our work, we translate complex scenes represented using meshes to acoustic IRs represented as audio signals.

3.2 TRAINING DATASET

In our work, we train MESH2IR on the GWA IR dataset [73] simulated using a hybrid algorithm to generate realistic IRs on unseen complex environments. The IRs in GWA are created by automatically calibrating the ray energies simulated using the geometric acoustic method [74] with the wave effects simulated using finite-difference time-domain wave solver [10] to create high-quality low-frequency and high-frequency wave effects. The GWA dataset consists of 2 million IRs simulated on the indoor 3D environments represented as meshes in the 3D-FRONT dataset. Out of the 2 million IRs, we train MESH2IR on 200,000 IRs simulated in 5,000 different indoor environments from 3D-FRONT dataset [21].

3.3 MESH SIMPLIFICATION

The number of faces in the 3D-FRONT dataset varies from about 2000 faces to 3 million faces. We initially simplify the meshes using a quadratic-based edge collapse algorithm in PyMeshLab [51] to have a fewer number of faces (i.e., 2000 faces). The edge collapse algorithm makes sure that the approximation error between the original mesh and the simplified mesh, in terms of Hausdorff distance is small. Therefore the acoustic characteristics do not change due to the simplification step.

Figure 3 depicts an example of the original indoor 3D scene mesh and the simplified mesh using the quadratic edge collapse algorithm. We can see that high-level details of the furniture such as bed, pillow, settee, table and cupboard are preserved in the simplified mesh, in addition to the scene geometry. In this example, the simplified mesh has only 2% of faces of the original mesh.

3.4 MESH ENCODER

Our goal is to transform the simplified indoor scene meshes into a low-dimensional latent space. The triangular meshes can be represented as graph data. Therefore, we represent the 3D scene meshes as a graph and use a graph network (Figure 2) to reduce the dimension. Our graph network uses graph convolution (GCN) layers [35]

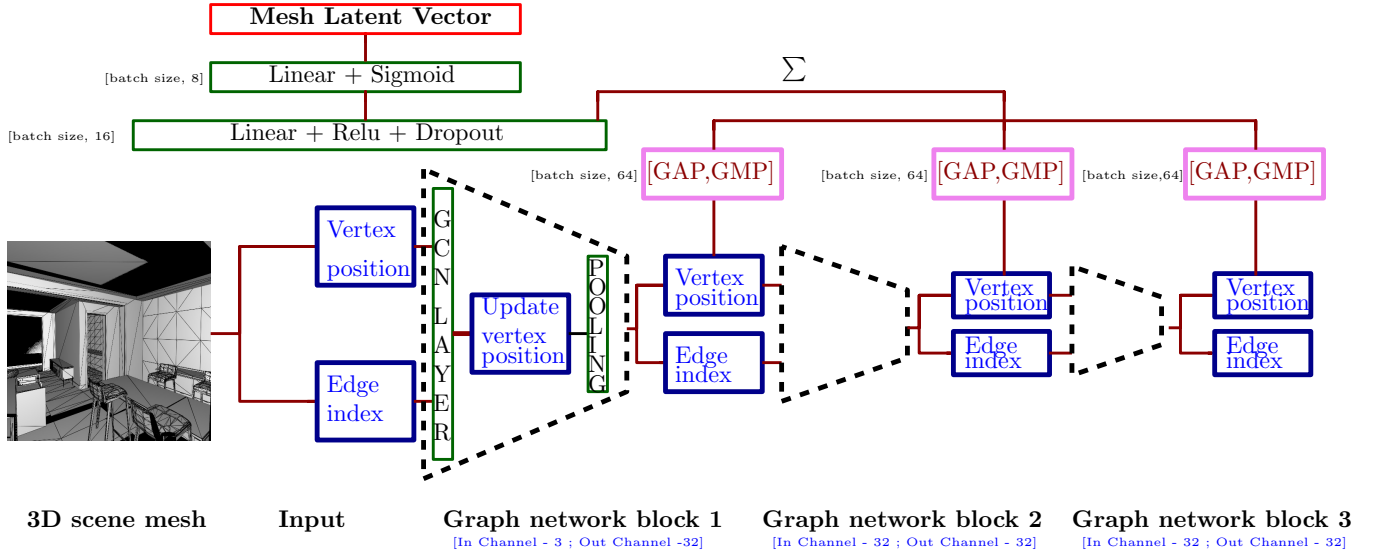


Figure 2: The expansion of our mesh encoder in Figure 1. Our encoder network transforms the indoor 3D scene mesh into a latent vector. The topology information (edge connectivity) and the node features (vertex coordinates) are extracted from the mesh and passed to our graph neural network.

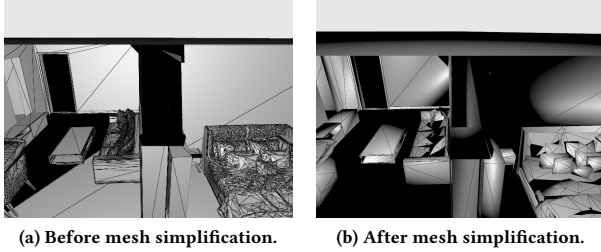


Figure 3: The indoor 3D scene is represented using an original mesh with around 100,000 faces and a simplified mesh with 2,000 faces. We can see that high-level details of the room geometry and furniture are preserved in the simplified mesh.

to encode the topology information (i.e., edge connectivity) and node features (i.e., vertex coordinates) of the graph. We use graph pooling (gpool) layers [22, 36] to reduce the topology information of the graph.

The layer-wise propagation rule of multi-layer GCN [35]:

$$X^{(l+1)} = \sigma(\hat{D}^{-\frac{1}{2}} \hat{A} \hat{D}^{-\frac{1}{2}} X^{(l)} W^{(l)}), \quad (2)$$

where $\hat{D}_{ii} = \sum_j \hat{A}_{ij}$, and $\hat{A} = A + I$. A is the adjacency matrix, I is the identity matrix and $W^{(l)}$ is a trainable weight matrix for layer l . The feature matrices at layers l and $l + 1$ are $X^{(l)}$ and $X^{(l+1)}$, respectively. The topology information is not modified in the GCN layer.

The gpool layer [22] creates a new graph with high-level feature encoding by choosing K vertices from the original vertex set and

discarding the other vertices. Some edges are removed when discarding vertices in the gpool layer. This results in some isolated vertices in the graph. To address this problem, the gpool algorithm increases the graph connectivity by calculating the square of the adjacency matrix $A^{(l)}$ at layer l and uses the new adjacency matrix $A_n^{(l)}$ for gpool computation (Equation 3).

$$A_n^{(l)} = A^{(l)} A^{(l)}. \quad (3)$$

We calculate the channel-wise average (GAP) and the channel-wise maximum (GMP) of the node features after each gpool layer and aggregate the GAP and GMP values. We concatenate the aggregated GAP and aggregated GMP values, pass them to linear layers, and get the mesh latent vector (π_M) (dimension=8) as the output.

3.5 SCENE VECTOR EMBEDDING

We concatenate the mesh latent vector (π_M) with the source (SP) and listener positions (LP) in 3D Cartesian space to generate scene vector embedding π_A of dimension 14 (Equation 4). The mesh latent vector will be learned during training.

$$\pi_A = [\pi_M \ SP \ LP]. \quad (4)$$

3.6 IR REPRESENTATION & PREPROCESSING

The IRs in the GWA dataset [73] have a sampling rate of 48 kHz. We downsample the IRs in the dataset to 16 kHz and crop the IRs. Downsampling IRs allows us to maintain a longer duration of IRs in a fixed-length input IR vector (3968 samples). The IRs with full duration and the IRs cropped to have a duration of around 0.25 seconds give similar performance in speech applications [61].

IR preprocessing: The IRs in the GWA dataset have large variations in standard deviation (STD) of the magnitude values (10^{-12} to 10^{-2}). We noticed that it is hard for MESH2IR to learn from such datasets with high dynamic ranges. To overcome this issue, we divide the IRs by ten times the STD to create preprocessed IRs with the same STD of 0.1 (or any constant STD). We noticed that preprocessing IRs to have constant STD improves the accuracy of MESH2IR (see Section 4.1).

To recover the IR with the original magnitude, we duplicate the STD of the IRs 128 times and concatenate them at the end of the preprocessed IRs. The concatenated IRs will have a length of 4096 ($3968+128$). The convolution layers in MESH2IR calculate an average of 41 neighboring sample values for each sample of the concatenated IRs and pass them to the next layer. Therefore, concatenated STD values near the end of preprocessed IR magnitudes in a concatenated IR will be corrupted when we calculate the average and pass it to the next layers. We can recover the STD values from the tail-end of the concatenated IR where all the 41 neighboring samples are STD.

3.7 ENERGY DECAY RELIEF

The energy decay relief (EDR) obtained from the physics-based algorithm contains enough information to be converted into an “equivalent impulse response” [42]. Therefore, we use EDR in the cost function of our MESH2IR. Constraining the Generator network with additional information (i.e., EDR) helps the model to converge easily.

The energy decay curve (EDC) describes the energy remaining in the IR with respect to time [67]. When compared to the IR itself, the EDC decays more smoothly, and we can use it to measure IR acoustic metrics. The generalized EDC for multiple frequency bands is called EDR [34]. EDR is the total amount of energy remaining in the IR at time t_n seconds in a frequency band centered at f_k Hz:

$$EDR(t_n, f_k) = \sum_{m=n}^M |H(m, k)|^2. \quad (5)$$

In Equation 5, bin k of the short-time Fourier transform at time-frame m is denoted by $H(m, k)$. M is the total number of time frames.

3.8 MODIFIED CONDITIONAL GAN

Our MESH2IR passes the scene vector embedding π_A (Equation 4) to a one-dimensional modified conditional GAN (CGAN) architecture proposed in FAST-RIR [61] to generate a single precise IR for the given indoor 3D scene. CGAN [23, 50] is conditioned on a random noise z and on a condition y to generate multiple different outputs that satisfy the condition y . The modified CGAN is only conditioned on y to generate a single output.

MESH2IR consists of a generator network (G_n) and a discriminator network (D_n), which are alternately trained at each iteration. We train G_n and D_n using the IR samples from the data distribution p_{data} . The objective function of our generator network consists of modified CGAN error, EDR error, and mean square error (MSE). We train the discriminator network with a modified CGAN objective

function. For each π_A , we use the corresponding IRs in the GWA dataset [73] as the ground truth when training our network.

Modified CGAN Error (Generator Network): The CGAN error is used to generate IRs that are hard for the D_n to differentiate from the ground truth IRs.

$$\mathcal{L}_{CGAN} = \mathbb{E}_{\pi_A \sim p_{data}} [\log(1 - D_N(G_N(\pi_A)))]. \quad (6)$$

EDR Error: For each π_A , we calculate the EDR of the generated IR using our MESH2IR (E_N) and the ground truth IR (E_G). We calculate EDR at a set of frequency bands with center frequencies at 125 Hz, 250 Hz, 500 Hz, 1000 Hz, 2000 Hz, and 4000 Hz (B). We compare the E_N and E_G for each sample (s) as follows:

$$\mathcal{L}_{EDR} = \mathbb{E}_{\pi_A \sim p_{data}} [\mathbb{E}_{b \sim B} [\mathbb{E}[(E_N(\pi_A, b, s) - E_G(\pi_A, b, s))^2]]]. \quad (7)$$

The signal energy in high-frequency components of EDR is high when compared with the signal energy in low-frequency components of EDR in the training IR dataset [73]. Therefore, we give more weight to low-frequency components of EDR.

MSE Error: For each π_A , we compare the IR generated from MESH2IR (I_N) with the ground truth IR (I_G). We calculate the squared difference of each sample (s) in I_N and I_G as follows:

$$\mathcal{L}_{MSE} = \mathbb{E}_{\pi_A \sim p_{data}} [\mathbb{E}[(I_N(\pi_A, s) - I_G(\pi_A, s))^2]]. \quad (8)$$

The generator network (G_N) and the discriminator network (D_N) are trained to compete each other by minimizing the generator objective function \mathcal{L}_{G_N} (Equation 9) and maximizing the discriminator objective function \mathcal{L}_{D_N} (Equation 10). In Equation 9, the relative importance of the EDR error and MSE error are controlled using λ_{EDR} and λ_{MSE} respectively.

$$\mathcal{L}_{G_N} = \mathcal{L}_{CGAN} + \lambda_{EDR} \mathcal{L}_{EDR} + \lambda_{MSE} \mathcal{L}_{MSE}. \quad (9)$$


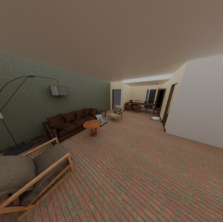
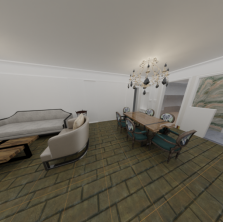

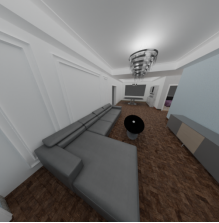
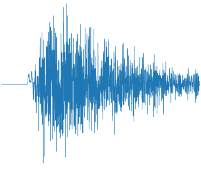
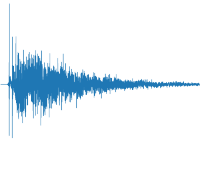
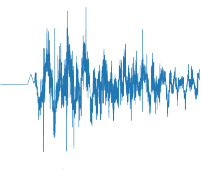
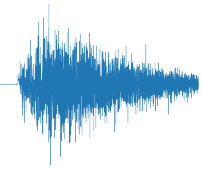
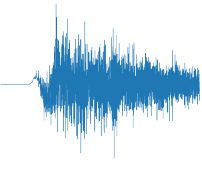
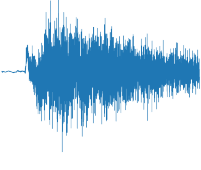
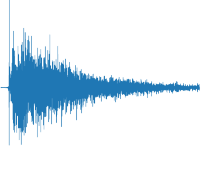
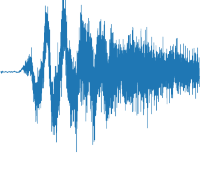
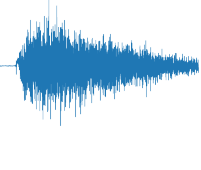
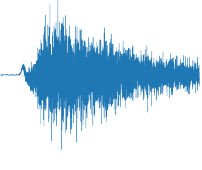
$$\mathcal{L}_{D_N} = \mathbb{E}_{(I_G, \pi_A) \sim p_{data}} [\log(D_N(I_G(\pi_A)))] + \mathbb{E}_{\pi_A \sim p_{data}} [\log(1 - D_N(G_N(\pi_A)))]. \quad (10)$$

3.9 IMPLEMENTATION DETAILS

Network Architecture: We adapt the graph encoder network in the PyG official repository [4] and modify the network to encode indoor 3D scene meshes to the latent space (Figure 2). Our pool layer keeps 60% of the original number of vertices in each layer. We use the Generator (G_N) network and the Discriminator network (D_N) architectures proposed in FAST-RIR [61] and modify their cost functions. We extend the G_N architecture proposed in FAST-RIR by adding our mesh encoder network (Figure 1).

Training: We trained G_N and D_N using the RMSprop optimizer with a batch size of 256. The G_N is iterated 3 times for every D_N iteration. Initially, we start with the learning rate of 8×10^{-5} and decay the learning rate by 85% of the original value for every 7 epochs. We trained our network for 150 epochs. We published our code for reproducibility at github [5].

Table 1: The accuracy of IRs generated using MESH2IR on 5 different furnished indoor 3D scenes not used for training. We plot the time-domain representation of ground truth IRs and the predicted IRs, and evaluate the accuracy of predicted IRs using relative reverberation time (T_{60}) error, relative direct-reverberant-ratio (DRR) error, and relative early-decay-time (EDT) error. Our MESH2IR can predict the IRs with less than 10% T_{60} and DRR errors, and less than 3% EDT error. We also can see that the envelope and magnitude of the predicted IRs matches the ground truth IRs.

Benchmark Scene					
# faces	185,319	92,422	181,536	253,684	282,375
Ground truth IR					
Our Mesh2IR					
T_{60} error	2.7%	5.9%	8.2%	0.6%	7.5%
DRR error	2.6%	9.4%	1.4%	1.9%	9.3%
EDT error	2.9%	2.1%	2.1%	1.7%	0.9%

4 ABLATION EXPERIMENTS

We perform an ablation study to analyze the importance of our IR preprocessing approach (Section 3.6) and to find an efficient way of adding EDR to the cost function. We quantitatively evaluate different variations of our network by calculating the mean absolute difference of different acoustic metrics of the generated IRs and the ground truth IRs. The acoustic characteristics of the 3D indoor environment are described using acoustic metrics [11]. We also measure the mean square error (MSE) of the generated IRs and the ground truth IRs (Equation 8). We train all the variations of our network with 200K IRs from 5000 different indoor 3D scene meshes and generate 11K testing IRs from 600 scene meshes not used during training. We use commonly-used acoustic metrics such as reverberation time (T_{60}), early-decay-time (EDT), and direct-to-reverberant ratio (DRR) in our experiment. The time taken to decay the sound pressure by 60 decibels (dB) is called T_{60} . DRR is the ratio of the sound pressure level of the direct sound to the sound pressure level of reflected sound [53]. EDT is six times the time taken for the sound source to decay by 10 dB, and it depends on the type and location of the sound source.

4.1 IR PREPROCESSING

We evaluate the contribution of our IR preprocessing approach discussed in Section 3.6. We train our MESH2IR on IRs without IR preprocessing (MESH2IR-UNPROCESSED) and generate IRs from our trained network. Figure 4 shows a ground truth IR and the IR generated from MESH2IR-UNPROCESSED. We can see that MESH2IR-UNPROCESSED generates noisy output. In Table 1 we can see that MESH2IR estimates the IRs for the given 3D scene to a greater extent.

4.2 ENERGY DECAY RELIEF (EDR)

To evaluate the importance and the efficient way of adding EDR to the cost functions, we train and compare two different variations of our MESH2IR network.

Variation 1 (MESH2IR-NO-EDR): We evaluate the role played by the EDR loss in the generator network by training a variant of MESH2IR without the EDR loss (Equation 7).

Variation 2 (MESH2IR-D-EDR): Instead of training the Discriminator network to discriminate between generated IRs and ground truth IRs of dimension 3968×1 , we train the Discriminator network to discriminate between the EDR of the generated IRs and

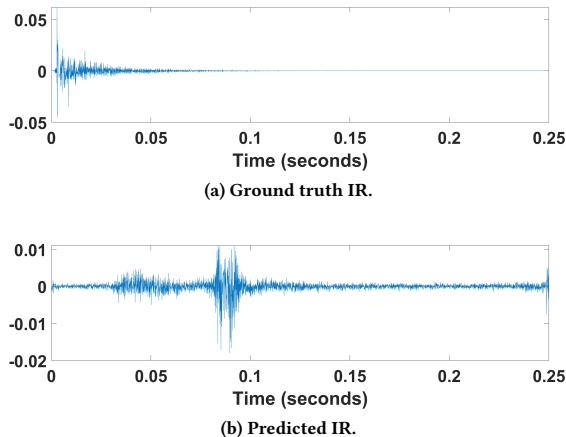


Figure 4: The ground truth IR, and the IR predicted by MESH2IR trained with an unprocessed IR training set (MESH2IR-UNPROCESSED). We can see that MESH2IR-UNPROCESSED gives noisy output.

Table 2: Mean absolute error of the acoustic metrics and mean square error of the generated IRs from MESH2IR-NO-EDR, MESH2IR-D-EDR and MESH2IR. The acoustic metrics used in our experiments are reverberation time (T_{60}) measured in seconds, direct-to-reverberant ratio (DRR) measured in decibels and early-decay-time (EDT) measured in seconds. We can see that overall MESH2IR gives the least error. The best results of each metric are "bolded".

IR Dataset	Mean Absolute Error ↓			MSE ($\times 10^{-4}$) ↓
	T_{60}	DRR	EDT	
MESH2IR-NO-EDR	0.16	2.68	0.23	1.44
MESH2IR-D-EDR	0.13	2.74	0.22	1.23
MESH2IR	0.13	2.72	0.22	1.23

the ground truth IRs. EDR is calculated at six octave bands with center frequencies at 125 Hz, 250 Hz, 500 Hz, 1000 Hz, 2000 Hz and 4000 Hz. The EDR of an IR has a dimension of 3986x6. We also train the Generator network with the EDR loss.

From Table 2, we can see that adding EDR in the generator loss function improves the T_{60} , EDT, and MSE. Training the Discriminator network with IRs (MESH2IR) gives a similar performance to passing EDR of the IRs (MESH2IR-D-EDR).

4.3 POWER SPECTRUM

The power spectrum describes the energy distribution of the IR in the frequency components that compose the waveform. In Figure 5, we compare the power spectrum of ground truth IRs with the power spectrum of the predicted IR using MESH2IR, MESH2IR-D-EDR, and MESH2IR-NO-EDR. In this example, we placed the listener 1m and 8m away from the source. We can see that in both cases the

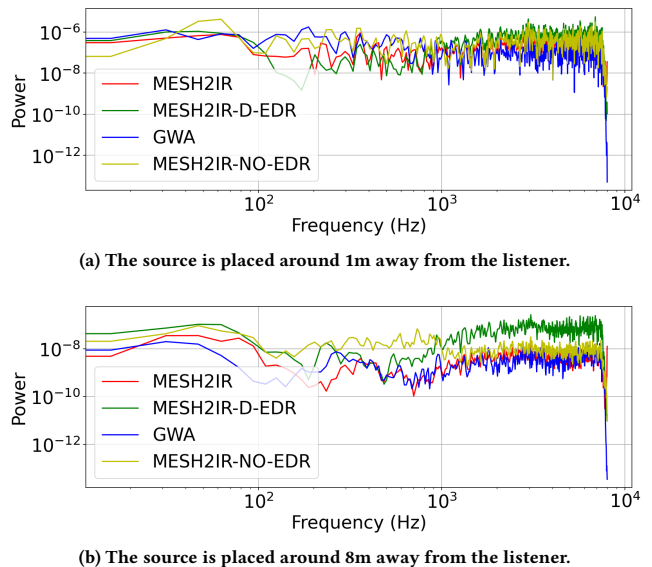


Figure 5: The power spectrum of IRs generated using our proposed MESH2IR, MESH2IR-D-EDR, MESH2IR-NO-EDR, and the ground truth IRs from the GWA dataset. We can see that the power spectrum of MESH2IR is closest to the power spectrum of GWA.

power spectrum of MESH2IR is closer to GWA when compared with other variants of our approach.

5 ACOUSTIC EVALUATION

In this section, we evaluate the accuracy, power spectrum and runtime of our MESH2IR network. We evaluate the accuracy of our MESH2IR network by comparing the relative acoustic metric error values of the IRs predicted from MESH2IR on indoor 3D scenes not used during training and the ground truth IRs from the GWA dataset [73]. We compare the run-time of MESH2IR network with a state-of-the-art geometric acoustic simulator [74].

5.1 ACCURACY ANALYSIS

To evaluate the robustness of our MESH2IR, we selected ground truth IRs from the GWA dataset [73] from 5 different indoor 3D scenes with different levels of complexity (the number of faces in a 3D scene mesh). The selected IRs have a large variation in magnitudes and shapes. The distance between the listener and the source position varies from 3.6m to 10.5m. We predicted IRs corresponding to the ground truth IRs in 3D scenes using our MESH2IR. We evaluate the accuracy of our prediction using relative T_{60} error, relative DRR error, and relative EDT error. Table 1 shows the ground truth IRs, predicted IRs and the accuracy of our prediction. We can see that our approach can predict the IRs with less than 10% T_{60} and DRR errors, and less than 3% EDT error, which are significantly lower than their just-noticeable-differences (JNDs) [9, 19, 78].

5.2 RUNTIME

We compare the runtime for generating 30,000 IRs from our MESH2IR with the time required to generate these samples from a geometric-based acoustic simulator (GA) [74] and FAST-RIR [61]. The runtime of GA depends on the complexity of the scene, and FAST-RIR is only capable of generating IRs for empty shoe-box-shaped medium-sized rooms (i.e., room dimensions varying from [8m,6m,2.5m] to [11m,8m,3.5m]). We compare the runtime of GA and FAST-RIR given in Ratnarajah et al. [61] with the runtime of MESH2IR for generating IRs for furnished indoor 3D scene meshes in the 3D-Front dataset [21]. We use an Intel(R) Xenon(R) CPU E52699 v4 @ 2.20 GHz and a GeForce RTX 2080 Ti GPU for our evaluation.

For a fair comparison with GA and FAST-RIR methods, which take 3D room dimensions as inputs, we did not consider the time taken for mesh simplification and mesh-to-graph conversion in Table 3. On average, mesh simplification takes around 7.5 seconds and mesh-to-graph conversion takes 0.04 seconds. From Table 3, we can see that MESH2IR is more than 200 times faster than GA on a CPU. MESH2IR is optimized to run on GPUs and supports batch parallelization. MESH2IR is slower than FAST-RIR because we encode a 3D scene mesh represented using a graph to a mesh latent vector using our graph neural network (Figure 2). To generate thousands of IRs for a given furnished indoor 3D scene, we perform mesh simplification, mesh-to-graph conversion, and mesh encoding only once.

We have shown the average time taken for mesh encoding (MESH2IR[Mesh Encoder]) and IR generation using the encoded mesh (MESH2IR[IR Generator]) separately in Table 3. Our MESH2IR can generate more than 10,000 IRs per second on a single GPU for a given furnished indoor 3D scene, and the runtime of MESH2IR is stable irrespective of the scene.

6 APPLICATIONS

We demonstrate the benefit of our MESH2IR for several downstream speech applications - neural sound rendering, speech dereverberation and reverberant speech separation. For a fair comparison between different methods, we generate 11K IRs from 600 scene meshes not used during training our MESH2IR using GA [74], GWA [73], MESH2IR-D-EDR, and MESH2IR. We generate reverberant speech using the 11K IRs, and train speech dereverberation and speech separation methods. Reverberant speech can be generated from a dry sound source and an IR via a convolution:

$$x(t) = s(t) * r(t) \quad (11)$$

where $x(t)$ is the reverberant speech signal, $r(t)$ is the IR, $s(t)$ is the dry speech signal.

6.1 NEURAL SOUND RENDERING

Our MESH2IR is the first neural-network-based approach to predict IRs from a given 3D scene mesh at interactive rates. Given this advantage, MESH2IR can be applied to general 3D scenes to enable real-time neural sound rendering, without pre-computation on new scenes. For single IR updates in dynamic scenes, MESH2IR can operate at more than 100 frames per second (fps), which is significantly beyond the requirement for interactive applications

Table 3: The runtime of a geometric acoustic simulator (GA) [74], FAST-RIR [61], and our MESH2IR. MESH2IR is an extension of FAST-RIR to generate IRs for complex indoor scenes. We can see that the runtime of MESH2IR is higher than FAST-RIR because we use a graph-based network to process the mesh. MESH2IR still outperforms GA on a single CPU.

IR Generator	Hardware	Avg time	Scene Type
GA [74]	CPU	30.05s	Simple
MESH2IR	CPU	0.13s	Complex
MESH2IR(Batch Size 1)	GPU	1.32×10^{-2} s	Complex
FAST-RIR(Batch Size 128)	GPU	5.9×10^{-5} s	Simple
MESH2IR(Batch Size 128)	GPU	2.6×10^{-3}s	Complex
MESH2IR[Mesh Encoder]	GPU	2.57×10^{-3}s	Complex
MESH2IR[IR Generator]	GPU	7.4×10^{-5}s	Complex

(e.g., 10 fps). We demonstrate its sound rendering quality in our supplemental video ¹.

6.2 SPEECH DEREVERBERATION

Speech dereverberation is the process of obtaining reverb-free speech from reverberant speech. We train speech dereverberation models using data generated from different synthetic IR generation methods and compare their performance on data generated from recorded IRs. We test the models on IRs from the MIT IR dataset [76], the BUTReverb dataset [72], and the RWCP Aachen IR dataset [30, 52]. For all experiments, we train the SkipConvNet [39] model with its default parameters. We use the metric speech-to-reverberation modulation energy ratio (SRMR) [20] to measure the improvement obtained by the dereverberation process. Higher SRMR implies higher speech quality and lower reverberation effects. We also report the SRMR of the baseline where we do not apply any dereverberation (Reverb).

In Table 4, we test the models on reverberant data generated from recorded IRs. Across all IR datasets, we see that the SRMR of our MESH2IR model is similar to the SRMR of the GWA IRs [73]. We also see that MESH2IR outperforms the GA [74] method, which only generates IRs using geometric simulations (less accurate than IRs generated from the GWA dataset). The SRMR of MESH2IR is closer to GWA IRs when compared with MESH2IR-D-EDR. Therefore, MESH2IR generates more accurate IRs when compared with MESH2IR-D-EDR.

6.3 SPEECH SEPARATION

Speech separation, also referred to as the cocktail party problem, is the process of separating a mixture of speech signals into its constituent speech signals. We check the performance of different synthetic IR generation methods on the task of reverberant speech separation - separating a reverberant mixture into its constituent reverberant speech signals. The dry speech signals and mixtures from the Libri2Mix [17] dataset are convolved with IRs to generate the reverberant data. We train the DPRNN-TasNet [46] model for all

¹<https://anton-jeran.github.io/M2IR/>

Table 4: Speech dereverberation results are obtained when training data is generated by different synthetic IR generation methods. Testing is done on reverberant data synthesized from IRs present in three different datasets containing recorded IRs collected in a variety of environments. Higher SRMR is better.

Training Dataset	SRMR		
	MIT	BUTReverb	RWCP Aachen
Reverb	7.35	3.14	5.16
GA [74]	6.39	3.74	4.83
GWA [73]	7.67	4.6	6.14
MESH2IR-D-EDR	6.18	3.29	4.32
MESH2IR (ours)	7.82	4.27	5.88

Table 5: Speech separation results in the presence of reverberation are shown below. We report the improvement in the Scale-Invariant Signal Distortion Ratio (SI-SDRi) over the reverberant mixture. Higher Si-SDRi is better. We report performance on reverberant mixtures generated in four different room configurations present in the VOICES dataset.

Training Dataset	SI-SDRi			
	Room 1	Room 2	Room 3	Room 4
GA [74]	2.26	2.22	1.33	2.35
GWA [73]	4.75	4.75	2.41	4.91
MESH2IR-D-EDR	4.68	4.35	1.87	4.72
MESH2IR (ours)	4.91	4.89	2.54	5.13

speech separation experiments. We utilize the default implementation provided by the Asteroid [56] framework. The model is tested on reverberant mixtures created from real recordings obtained from four different room configurations in the VOICES [63] dataset. We clearly see that our MESH2IR performs similar to GWA [73], and outperforms GA method [74] and MESH2IR-D-EDR.

7 CONCLUSION AND FUTURE WORK

We present a novel neural-network-based MESH2IR architecture to generate thousands of IRs for a given furnished indoor 3D scene on the fly. The IR generation speed of our MESH2IR is constant within a given complex 3D scene, irrespective of the complexity of the scene. Our MESH2IR can generate thousands of IRs per second for a given 3D scene. We show that the IRs predicted by our MESH2IR in unseen indoor 3D scenes are highly similar to the ground truth IRs generated from the GWA dataset, which is used to train our MESH2IR.

Our work has some limitations. One is we cannot control the characteristics of the scene materials such as the amount of sound absorption and scattering, which can affect the overall amplitude of the IR. Efficiently inputting the characteristics of scene material to our MESH2IR may improve the accuracy of IR generation. In addition, while MESH2IR can handle moving sound by simulating many IRs according to a trajectory, when objects in the scene moves, the scene representation changes, which incurs additional encoding time for MESH2IR, making it less efficient in highly dynamic scenes.

In the future, we would like to integrate our MESH2IR into game engines and other interactive applications, and evaluate its benefits.

REFERENCES

- [1] 2018. *Steam audio*. <https://valvesoftware.github.io/steam-audio/>
- [2] 2019. *Microsoft project acoustics*. <https://docs.microsoft.com/en-us/gaming/acoustics/what-is-acoustics>
- [3] 2019. *Oculus spatializer*. <https://developer.oculus.com/downloads/package/oculus-spatializer-unity/>
- [4] 2021. *PyG official repository: Proteins topk pool*. https://github.com/pyg-team/pytorch_geometric/blob/master/examples/proteins_topk_pool.py
- [5] 2022. *MESH2IR official repository*. <https://github.com/anton-jeran/MESH2IR>
- [6] Jont B. Allen and David A. Berkley. 1979. Image method for efficiently simulating small-room acoustics. *The Journal of the Acoustical Society of America* 65, 4 (1979), 943–950. <https://doi.org/10.1121/1.382599> arXiv:<https://doi.org/10.1121/1.382599>
- [7] Rohith Aralikatti, Anton Ratnarajah, Zhenyu Tang, and Dinesh Manocha. 2021. Improving Reverberant Speech Separation with Synthetic Room Impulse Responses. In *ASRU*. IEEE, 900–906.
- [8] Armen Avetisyan, Manuel Dahner, Angela Dai, Manolis Savva, Angel X. Chang, and Matthias Nießner. 2019. Scan2CAD: Learning CAD Model Alignment in RGB-D Scans. In *CVPR*. Computer Vision Foundation / IEEE, 2614–2623.
- [9] Matthew G Blevins, Adam T Buck, Zhao Peng, and Lily M Wang. 2013. Quantifying the just noticeable difference of reverberation time with band-limited noise centered around 1000 Hz using a transformed up-down adaptive method. (2013).
- [10] D. Botteldooren. 1995. Finite-difference time-domain simulation of low-frequency room acoustic problems. *The Journal of the Acoustical Society of America* 98, 6 (1995), 3302–3308. <https://doi.org/10.1121/1.413817> arXiv:<https://doi.org/10.1121/1.413817>
- [11] Nicholas J. Bryan. 2020. Impulse Response Data Augmentation and Deep Neural Networks for Blind Room Acoustic Parameter Estimation. In *ICASSP*. IEEE, 1–5.
- [12] Diego Di Carlo, Pinchas Tanditnik, Cédric Foy, Antoine Deleforge, Nancy Bertin, and Sharon Gannot. 2021. dEchorate: a Calibrated Room Impulse Response Database for Echo-aware Signal Processing. *CoRR* abs/2104.13168 (2021).
- [13] Angel X. Chang, Angela Dai, Thomas A. Funkhouser, Maciej Halber, Matthias Nießner, Manolis Savva, Shuran Song, Andy Zeng, and Yinda Zhang. 2017. Matterport3D: Learning from RGB-D Data in Indoor Environments. In *3DV*. IEEE Computer Society, 667–676.
- [14] Changan Chen, Ruohan Gao, Paul Calamia, and Kristen Grauman. 2022. Visual Acoustic Matching. *CoRR* abs/2202.06875 (2022).
- [15] Changan Chen, Unnat Jain, Carl Schissler, Sebastia Vicenc Amengual Gari, Ziad Al-Halah, Vamsi Krishna Ithapu, Philip Robinson, and Kristen Grauman. 2020. SoundSpaces: Audio-Visual Navigation in 3D Environments. In *ECCV*.
- [16] Changan Chen, Sagnik Majumder, Ziad Al-Halah, Ruohan Gao, Santhosh Kumar Ramakrishnan, and Kristen Grauman. 2021. Learning to Set Waypoints for Audio-Visual Navigation. In *ICLR*. OpenReview.net.
- [17] Joris Costentino, Manuel Pariente, Samuele Cornell, Antoine Deleforge, and Emmanuel Vincent. 2020. Librimix: An open-source dataset for generalizable speech separation. *arXiv preprint arXiv:2005.11262* (2020).
- [18] Angela Dai, Angel X. Chang, Manolis Savva, Maciej Halber, Thomas A. Funkhouser, and Matthias Nießner. 2017. ScanNet: Richly-Annotated 3D Reconstructions of Indoor Scenes. In *CVPR*. IEEE Computer Society, 2432–2443.
- [19] Fernando del Solar Dorrego and Michelle C Vigeant. 2022. A study of the just noticeable difference of early decay time for symphonic halls. *The Journal of the Acoustical Society of America* 151, 1 (2022), 80–94.
- [20] Tiago H Falk, Chenxi Zheng, and Wai-Yip Chan. 2010. A non-intrusive quality and intelligibility measure of reverberant and dereverberated speech. *IEEE Transactions on Audio, Speech, and Language Processing* 18, 7 (2010), 1766–1774.
- [21] Huan Fu, Bowen Cai, Lin Gao, Ling-Xiao Zhang, Jiaming Wang, Cao Li, Qixun Zeng, Chengyue Sun, Rongfei Jia, Binqiang Zhao, et al. 2021. 3d-front: 3d furnished rooms with layouts and semantics. In *Proceedings of the IEEE/CVF International Conference on Computer Vision*. 10933–10942.
- [22] Hongyang Gao and Shuiwang Ji. 2019. Graph U-Nets. In *ICML (Proceedings of Machine Learning Research, Vol. 97)*. PMLR, 2083–2092.
- [23] Jon Gauthier. 2015. Conditional generative adversarial networks for convolutional face generation. In *Tech Report*.
- [24] François Grondin, Jean-Samuel Lauzon, Simon Michaud, Mirco Ravanelli, and François Michaud. 2020. BIRD: Big Impulse Response Dataset. *CoRR* abs/2010.09930 (2020).
- [25] Pierre-Amaury Grumiaux, Srđan Kitić, Laurent Girin, and Alexandre Guérin. 2021. A Survey of Sound Source Localization with Deep Learning Methods. *CoRR* abs/2109.03465 (2021).
- [26] Elijor Hadad, Florian Heese, Peter Vary, and Sharon Gannot. 2014. Multichannel audio database in various acoustic environments. In *IWAENC*. IEEE, 313–317.
- [27] Ankur Handa, Viorica Patraucean, Vijay Badrinarayanan, Simon Stent, and Roberto Cipolla. 2015. SceneNet: Understanding Real World Indoor Scenes With Synthetic Data. *CoRR* abs/1511.07041 (2015).

- [28] Scott H Hawley, Vasileios Chatziannou, and Andrew Morrison. 2020. Synthesis of musical instrument sounds: Physics-based modeling or machine learning. *Phys. Today* 16 (2020), 20–28.
- [29] Teerapat Jenrungrot, Vivek Jayaram, Steven M. Seitz, and Ira Kemelmacher-Shlizerman. 2020. The Cone of Silence: Speech Separation by Localization. In *NeurIPS*.
- [30] Marco Jeub, Magnus Schafer, and Peter Vary. 2009. A binaural room impulse response database for the evaluation of dereverberation algorithms. In *2009 16th International Conference on Digital Signal Processing*. IEEE, 1–5.
- [31] Shulei Ji, Jing Luo, and Xinyu Yang. 2020. A Comprehensive Survey on Deep Music Generation: Multi-level Representations, Algorithms, Evaluations, and Future Directions. *arXiv preprint arXiv:2011.06801* (2020).
- [32] Xutong Jin, Sheng Li, Dinesh Manocha, and Guoping Wang. 2021. DeepEigen: Learning-based Modal Sound Synthesis with Acoustic Transfer Maps. *CoRR abs/2108.07425* (2021).
- [33] Xutong Jin, Sheng Li, Tianshu Qu, Dinesh Manocha, and Guoping Wang. 2020. Deep-modal: real-time impact sound synthesis for arbitrary shapes. In *Proceedings of the 28th ACM International Conference on Multimedia*. 1171–1179.
- [34] Jean-Marc Jot. 1992. An analysis/synthesis approach to real-time artificial reverberation. In *ICASSP*. IEEE Computer Society, 221–224.
- [35] Thomas N. Kipf and Max Welling. 2017. Semi-Supervised Classification with Graph Convolutional Networks. In *ICLR (Poster)*. OpenReview.net.
- [36] Boris Knyazev, Graham W. Taylor, and Mohamed R. Amer. 2019. Understanding Attention and Generalization in Graph Neural Networks. In *NeurIPS*. 4204–4214.
- [37] Tom Ko, Vijayaditya Peddinti, Daniel Povey, Michael L. Seltzer, and Sanjeev Khudanpur. 2017. A study on data augmentation of reverberant speech for robust speech recognition. In *ICASSP*. IEEE, 5220–5224.
- [38] homare kon and hideki koike. 2019. estimation of late reverberation characteristics from a single two-dimensional environmental image using convolutional neural networks. *journal of the audio engineering society* 67, 7/8 (july 2019), 540–548. <https://doi.org/10.17743/jaes.2018.0069>
- [39] Vinay Kothapally, Wei Xia, Shahram Ghorbani, John HL Hansen, Wei Xue, and Jing Huang. 2020. Skipconvnet: Skip convolutional neural network for speech dereverberation using optimally smoothed spectral mapping. *arXiv preprint arXiv:2007.09131* (2020).
- [40] Shoichi Koyama, Tomoya Nishida, Keisuke Kimura, Takumi Abe, Natsuki Ueno, and Jesper Brunnström. 2021. MESHRIR: A Dataset of Room Impulse Responses on Meshed Grid Points for Evaluating Sound Field Analysis and Synthesis Methods. In *WASPAA*. IEEE, 1–5.
- [41] Heinrich Kuttruff. 2016. *Room acoustics*. Crc Press.
- [42] k. heinrich kuttruff. 1993. auralization of impulse responses modeled on the basis of ray-tracing results. *journal of the audio engineering society* 41, 11 (november 1993), 876–880.
- [43] Tobias Lentz, Dirk Schröder, Michael Vorländer, and Ingo Assenmacher. 2007. Virtual Reality System with Integrated Sound Field Simulation and Reproduction. *EURASIP J. Adv. Signal Process* 2007, 1 (jan 2007), 187. <https://doi.org/10.1155/2007/70540>
- [44] Shiguang Liu and Dinesh Manocha. 2020. Sound Synthesis, Propagation, and Rendering: A Survey. *CoRR abs/2011.05538* (2020).
- [45] Andrew Luo, Yilun Du, Michael J. Tarr, Joshua B. Tenenbaum, Antonio Torralba, and Chuang Gan. 2022. Learning Neural Acoustic Fields. *CoRR abs/2204.00628* (2022).
- [46] Yi Luo, Zhuo Chen, and Takuya Yoshioka. 2020. Dual-path rnn: efficient long sequence modeling for time-domain single-channel speech separation. In *ICASSP 2020-2020 IEEE International Conference on Acoustics, Speech and Signal Processing (ICASSP)*. IEEE, 46–50.
- [47] Mishaim Malik, Muhammad Kamran Malik, Khawar Mehmood, and Imran Makhdoom. 2021. Automatic speech recognition: a survey. *Multim. Tools Appl.* 80, 6 (2021), 9411–9457.
- [48] Ravish Mehra, Nikunj Raghuvanshi, Lakulish Antani, Anish Chandak, Sean Curtis, and Dinesh Manocha. 2013. Wave-Based Sound Propagation in Large Open Scenes Using an Equivalent Source Formulation. *ACM Trans. Graph.* 32, 2, Article 19 (apr 2013), 13 pages. <https://doi.org/10.1145/2451236.2451245>
- [49] Hsien-Yu Meng, Zhenyu Tang, and Dinesh Manocha. 2021. Point-based Acoustic Scattering for Interactive Sound Propagation via Surface Encoding. In *IJCAI*. ijcai.org, 909–915.
- [50] Mehdi Mirza and Simon Osindero. 2014. Conditional Generative Adversarial Nets. *arXiv preprint arXiv:1411.1784* (2014).
- [51] Alessandro Muntoni and Paolo Cignoni. 2021. *PyMeshLab*. <https://doi.org/10.5281/zenodo.4438750>
- [52] Satoshi Nakamura, Kazuo Hiyané, Futoshi Asano, and Takashi Endo. 1999. Sound scene data collection in real acoustical environments. *Journal of the Acoustical Society of Japan (E)* 20, 3 (1999), 225–231.
- [53] P A Naylor and N D Gaubitch. 2010. *Speech Dereverberation* (1st ed.). Springer Publishing Company, Incorporated.
- [54] Vincent W. Neo, Christine Evers, and Patrick A. Naylor. 2020. PEVD-Based Speech Enhancement in Reverberant Environments. In *ICASSP*. IEEE, 186–190.
- [55] Andrew Owens, Phillip Isola, Josh H. McDermott, Antonio Torralba, Edward H. Adelson, and William T. Freeman. 2016. Visually Indicated Sounds. In *CVPR*. IEEE Computer Society, 2405–2413.
- [56] Manuel Pariente, Samuele Cornell, Joris Cosentino, Sunit Sivasankaran, Efthymios Tzinis, Jens Heitkaemper, Michel Olvera, Fabian-Robert Stöter, Mathieu Hu, Juan M Martín-Doñas, et al. 2020. Asteroid: the PyTorch-based audio source separation toolkit for researchers. *arXiv preprint arXiv:2005.04132* (2020).
- [57] Ville Pulkki and U. Peter Svensson. 2019. Machine-learning-based estimation and rendering of scattering in virtual reality. *The Journal of the Acoustical Society of America* 145, 4 (2019), 2664–2676. <https://doi.org/10.1121/1.5095875>
- [58] Nikunj Raghuvanshi, John Snyder, Ravish Mehra, Ming Lin, and Naga Govindaraju. 2010. Precomputed Wave Simulation for Real-Time Sound Propagation of Dynamic Sources in Complex Scenes. *ACM Trans. Graph.* 29, 4, Article 68 (jul 2010), 11 pages. <https://doi.org/10.1145/1778765.1778805>
- [59] Anton Ratnarajah, Zhenyu Tang, and Dinesh Manocha. 2021. IR-GAN: Room Impulse Response Generator for Far-Field Speech Recognition. In *Proc. Interspeech 2021*. 286–290. <https://doi.org/10.21437/Interspeech.2021-230>
- [60] Anton Ratnarajah, Zhenyu Tang, and Dinesh Manocha. 2021. TS-RIR: Translated Synthetic Room Impulse Responses for Speech Augmentation. In *ASRU*. IEEE, 259–266.
- [61] Anton Ratnarajah, Shi-Xiong Zhang, Meng Yu, Zhenyu Tang, Dinesh Manocha, and Dong Yu. 2021. FAST-RIR: Fast neural diffuse room impulse response generator. *CoRR abs/2110.04057* (2021).
- [62] Alexander Richard, Peter Dodds, and Vamsi Krishna Ithapu. 2022. Deep Impulse Responses: Estimating and Parameterizing Filters with Deep Networks. *CoRR abs/2202.03416* (2022).
- [63] Colleen Richey, Maria A Barrios, Zeb Armstrong, Chris Bartels, Horacio Franco, Martin Graciarena, Aaron Lawson, Mahesh Kumar Nandwana, Allen Stauffer, Julien van Hout, et al. 2018. Voices obscured in complex environmental settings (voices) corpus. *arXiv preprint arXiv:1804.05053* (2018).
- [64] Carl Schissler and Dinesh Manocha. 2011. GSound: Interactive Sound Propagation for Games. *Journal of the audio engineering society* (February 2011).
- [65] Carl Schissler and Dinesh Manocha. 2016. Interactive Sound Propagation and Rendering for Large Multi-Source Scenes. *ACM Trans. Graph.* 36, 4, Article 114c (sep 2016), 12 pages. <https://doi.org/10.1145/3072959.2943779>
- [66] Carl Schissler, Ravish Mehra, and Dinesh Manocha. 2014. High-Order Diffraction and Diffuse Reflections for Interactive Sound Propagation in Large Environments. *ACM Trans. Graph.* 33, 4, Article 39 (jul 2014), 12 pages. <https://doi.org/10.1145/2601097.2601216>
- [67] M. R. Schroeder. 1965. New Method of Measuring Reverberation Time. *The Journal of the Acoustical Society of America* 37, 6 (1965), 1187–1188. <https://doi.org/10.1121/1.1939454> [arXiv:https://doi.org/10.1121/1.1939454](https://doi.org/10.1121/1.1939454)
- [68] Yiwen Shao, Shi-Xiong Zhang, and Dong Yu. 2021. Multi-Channel Multi-Speaker ASR Using 3D Spatial Feature. *CoRR abs/2111.11023* (2021).
- [69] Nikhil Singh, Jeff Mentch, Jerry Ng, Matthew Beveridge, and Iddo Drori. 2021. Image2Reverb: Cross-Modal Reverb Impulse Response Synthesis. In *ICCV*. IEEE, 286–295.
- [70] Christian J. Steinmetz, Vamsi Krishna Ithapu, and Paul Calamia. 2021. Filtered Noise Shaping for Time Domain Room Impulse Response Estimation from Reverberant Speech. In *WASPAA*. IEEE, 221–225.
- [71] Igor Szöke, Miroslav Skácel, Ladislav Mosner, Jakub Paliesek, and Jan Honza Cernocký. 2019. Building and Evaluation of a Real Room Impulse Response Dataset. *IEEE J. Sel. Top. Signal Process.* 13, 4 (2019), 863–876.
- [72] Igor Szöke, Miroslav Skácel, Ladislav Mošner, Jakub Paliesek, and Jan Černocký. 2019. Building and evaluation of a real room impulse response dataset. *IEEE Journal of Selected Topics in Signal Processing* 13, 4 (2019), 863–876. <https://doi.org/10.1109/JSTSP.2019.2917582>
- [73] Zhenyu Tang, Rohith Aralikkatti, Anton Ratnarajah, and Dinesh Manocha. 2022. GWA: A Large High-Quality Acoustic Dataset for Audio Processing. *ArXiv abs/2204.01787* (2022).
- [74] Zhenyu Tang, Lianwu Chen, Bo Wu, Dong Yu, and Dinesh Manocha. 2020. Improving Reverberant Speech Training Using Diffuse Acoustic Simulation. In *ICASSP*. IEEE, 6969–6973.
- [75] Micah Taylor, Anish Chandak, Qi Mo, Christian Lauterbach, Carl Schissler, and Dinesh Manocha. 2012. Guided Multiview Ray Tracing for Fast Auralization. *IEEE Transactions on Visualization and Computer Graphics* 18, 11 (2012), 1797–1810. <https://doi.org/10.1109/TVCG.2012.27>
- [76] James Traer and Josh H McDermott. 2016. Statistics of natural reverberation enable perceptual separation of sound and space. *Proceedings of the National Academy of Sciences* 113, 48 (2016), E7856–E7865.
- [77] Nanyang Wang, Yinda Zhang, Zhuwen Li, Yanwei Fu, Wei Liu, and Yu-Gang Jiang. 2018. Pixel2Mesh: Generating 3D Mesh Models from Single RGB Images. In *ECCV (1) (Lecture Notes in Computer Science, Vol. 11215)*. Springer, 55–71.
- [78] Stephan Werner and Judith Liebetrau. 2014. Adjustment of direct-to-reverberant-energy-ratio and the just-noticeable-difference. In *2014 Sixth International Workshop on Quality of Multimedia Experience (QoMEX)*. IEEE, 1–3.

- [79] LC Wrobel. 2003. Boundary Element Method, Volume 1: Applications in Thermo-Fluids and Acoustics. *Applied Mechanics Reviews* 56, 2 (03 2003), B17–B17. <https://doi.org/10.1115/1.1553431>
- [80] Hengchin Yeh, Ravish Mehra, Zhimin Ren, Lakulish Antani, Dinesh Manocha, and Ming Lin. 2013. Wave-Ray Coupling for Interactive Sound Propagation in Large Complex Scenes. *ACM Trans. Graph.* 32, 6, Article 165 (nov 2013), 11 pages. <https://doi.org/10.1145/2508363.2508420>
- [81] Han Zhang, Tao Xu, Hongsheng Li, Shaoting Zhang, Xiaogang Wang, Xiaolei Huang, and Dimitris Metaxas. 2017. StackGAN: Text to Photo-realistic Image Synthesis with Stacked Generative Adversarial Networks. In *ICCV*.
- [82] Han Zhang, Tao Xu, Hongsheng Li, Shaoting Zhang, Xiaogang Wang, Xiaolei Huang, and Dimitris N. Metaxas. 2019. StackGAN++: Realistic Image Synthesis with Stacked Generative Adversarial Networks. *IEEE Trans. Pattern Anal. Mach. Intell.* 41, 8 (2019), 1947–1962.